⌘ *Author's Choice*

THE JOURNAL OF BIOLOGICAL CHEMISTRY VOL. 283, NO. 35, pp. 24077–24088, August 29, 2008

Crystal Structure of Soluble Domain of Malaria Sporozoite Protein UIS3 in Complex with Lipid*

Received for publication, March 11, 2008, and in revised form, June 23, 2008 Published, JBC Papers in Press, June 23, 2008, DOI 10.1074/jbc.M801946200

Ashwani Sharma[1], **M. Yogavel**[2], **Reetesh Raj Akhouri, Jasmita Gill**[2], **and Amit Sharma**[2,3]

From the Structural and Computational Biology Group, International Centre for Genetic Engineering and Biotechnology, New Delhi 110067, India

Malaria parasite *UIS3* (up-regulated in infective sporozoites gene 3) is essential for sporozoite development in infected hepatocytes. *UIS3* encodes for a membrane protein that is localized to the parasite parasitophorous vacuolar membrane in infected hepatocytes. We describe here 2.5-Å resolution crystal structure of *Plasmodium falciparum* UIS3 soluble domain (PfUIS3$^{130-229}$) in complex with the lipid phosphatidylethanolamine (PE). PfUIS3$^{130-229}$ is a novel, compact, and all α-helical structure bound to one molecule of PE. The PfUIS3$^{130-229}$-PE complex structure reveals a novel binding site with specific interactions between PfUIS3$^{130-229}$ and the PE head group. One acyl chain of PE wraps around part of PfUIS3$^{130-229}$ and docks onto a hydrophobic channel. We additionally provide new structural and biochemical evidence of PfUIS3$^{130-229}$ interactions with lipids (phosphatidylethanolamine), with phospholipid liposomes, and with the human liver fatty acid-binding protein. The direct interaction of PfUIS3$^{130-229}$ with liver fatty acid-binding protein most likely provides the parasite with a conduit for importing essential fatty acids/lipids. Therefore, our analyses have implications for lipid transport into the parasite during the rapid growth phases of sporozoites. Given that PfUIS3 is essential for establishment of liver stage infection by *P. falciparum*, our data provide a new target for abrogating parasite development within liver cells before typical symptoms of malaria can manifest.

Plasmodium parasites are causative agents of malaria, which affects >500 million people and claims ~2 million lives annually (1). Rapid development of drug-resistant parasites and insecticide-resistant vectors necessitates discovery of novel drug and vaccine targets. Malaria infection is initiated in a human host when an infected *Anopheles* mosquito injects invasive sporozoites via the skin during a blood meal. Differential transcriptome profiling has identified ~25 *Plasmodium* genes that are specifically up-regulated in invasive sporozoites (2). Two such genes, called *UIS3* and *UIS4*, are critical for the establishment of blood stage infection in *Plasmodium* parasites (3). *UIS3*-deficient parasites can start the transformation process in the liver; however, they show severe defects during transformation into trophozoites. Parasites lacking the gene for *UIS3* are also unable to develop into mature liver schizonts and therefore abort malaria infection within the liver itself (3). Crucially, immunization with *UIS3*-deficient sporozoites imparts complete protection against malaria in the rodent malaria model (3).

UIS3 gene encodes a malaria parasite specific, unique, membrane-bound protein localized to the sporozoite parasitophorous vacuolar membrane (PVM)[4] (4). The latter is a membranous network that surrounds the intracellular parasite, and it differs substantially from other membranous compartments like endosomes or phagolysosomes (5). Interestingly, most of the fatty acids and lipids in the parasite PVM arise from the host cell, thus highlighting the fact that fatty acid/lipid import is crucial for parasite growth (5). The PVM is further modified by insertion of parasite-encoded proteins (including UIS3 and UIS4), which together may regulate various transport activities between parasite and the host cytoplasm (4). UIS3 appears to play a central role in fatty acid/lipid import during phases of rapid parasite growth (4). The severe developmental defects evident in *UIS3*-deficient malaria parasites provide a rationale for dissecting the biochemical and structural attributes of UIS3. Abrogation of parasite growth and developmental arrest during the liver stages of malaria infection, by design of unique antimalarials that target the pathologically silent liver stages of the malaria life cycle, deserves renewed attention.

Studies using the yeast two-hybrid system and co-immunoprecipitation experiments have recently suggested that *Plasmodium yoelii* UIS3 protein is capable of binding to the mouse liver fatty acid-binding protein (LFABP) (4). Down-regulation of mouse LFABP severely impaired development of rodent malaria parasites (4). These data argue that delivery of fatty acid/lipid cargo from LFABP to UIS3 protein may be an important pathway for fatty acid/lipid import into the parasite. Mem-

* This work is supported by a Department of Biotechnology (Government of India) career development award (to A. S.). The costs of publication of this article were defrayed in part by the payment of page charges. This article must therefore be hereby marked "*advertisement*" in accordance with 18 U.S.C. Section 1734 solely to indicate this fact.

⌘ *Author's Choice*—Final version full access.

The atomic coordinates and structure factors (code 2vwa) have been deposited in the Protein Data Bank, Research Collaboratory for Structural Bioinformatics, Rutgers University, New Brunswick, NJ (http://www.rcsb.org/).

[1] Supported by a University Grants Commission Government of India fellowship.

[2] Supported by the Wellcome Trust.

[3] International Wellcome Trust Senior Research Fellow in Biomedical Sciences. To whom correspondence should be addressed: International Centre for Genetic Engineering and Biotechnology, Aruna Asaf Ali Road, New Delhi 110067, India. Tel./Fax: 91-11-26741731; E-mail: amit.icgeb@gmail.com.

[4] The abbreviations used are: PVM, parasitophorous vacuolar membrane; PE, phosphatidylethanolamine; LFABP, fatty acid-binding protein; LFABP, liver FABP; GST, glutathione *S*-transferase; PBS, phosphate-buffered saline; MES, 4-morpholineethanesulfonic acid; BSA, bovine serum albumin; ELISA, enzyme-linked immunosorbent assay; MS, mass spectrometry.

bers of the fatty acid-binding protein (FABP) family typically show affinity for both saturated and unsaturated fatty acids (6). The LFABP differs from other members of FABP family in regards to its ligand binding stoichiometry (it can bind two independent chains of fatty acids) and in its ability to bind a spectrum of hydrophobic ligands (7–9). Intracellular FABPs are composed of 10 stranded anti-parallel β-barrels with two short anti-parallel α-helices positioned over one end of the β-barrel (10). The crystal structure of rat LFABP reveals the same conserved FABP fold but with structural differences that dramatically alter ligand specificities (6). Rat LFABP possesses two ligand-binding sites in different environments in terms of fatty acid burial within the protein (6). Crucially, the carboxylate group of second oleate in LFABP appears to be fully solvent-accessible (6). The liver FABPs are also capable of interacting with lysophospholipids in a stoichiometric ratio of 1:1.

The obligate nature of *UIS3* gene for sporozoite development and interaction of UIS3 with LFABP together suggest parasite reliance on fatty acid/lipid acquisition from host hepatocytes (4). The rapidly growing population of liver stage parasites probably requires excessive amounts of lipids for membrane biogenesis, and UIS3-LFABP cross-talk may provide such conduits. We present here a detailed structure-function dissection of the PfUIS3$^{130-229}$-phosphatidylethanolamine complex and provide evidence for direct interaction of PfUIS3$^{130-229}$ with phospholipid vesicles and with human LFABP. These studies lay a foundation for the development of specific inhibitors that may block development of the parasite in infected host liver before pathological symptoms of malaria infection appear.

EXPERIMENTAL PROCEDURES

Molecular Cloning, Expression, and Purification of PfUIS3—The *UIS3* gene from *Plasmodium falciparum* (GenBank™ accession number XM_001349714; PlasmoDB number PF13_0012) was PCR-amplified from a sporozoite cDNA library. The amplified fragment (residues 83–229) was cloned between BamHI and SalI restriction sites in pGEX4T1 vector and the protein expressed in fusion with GST. For production of selenium-methionine-labeled protein, *Escherhichia coli* B834 (DE3) cells were freshly transformed, and a single colony was grown in 10 ml of minimal medium supplemented with 0.2% (w/v) glucose, 50 μg ml^{-1} carbenicillin, and all amino acids including selenomethionine (except Met and Cys) (11). After 24 h of growth, this seed culture was used to inoculate a 1-liter culture that was grown for 20 h at 37 °C. Protein expression was induced by the addition of 1 mM isopropyl β-D-thiogalactopyranoside, and the culture was grown for 12 h post-induction. The resulting bacterial pellet from this 1-liter culture was suspended in 40 ml of PBS, pH 7.4, supplemented with lysozyme (100 μg ml^{-1}) and protease inhibitor mixture. The cells were sonicated and cleared by centrifugation at 20,000 $\times$ *g*. The cleared supernatant was passed through glutathione-Sepharose beads, which were then washed with PBS to remove impurities. PfUIS3-GST fusion protein was directly subjected to thrombin cleavage at 20 °C for 8 h on the beads. Cleaved PfUIS3 protein was subsequently collected as flow through, and the thrombin in solution was inactivated by benzamidine treatment (final concentration, 2 mM). Eluted PfUIS3 was concentrated using a 5-kDa Centricon (Viva Biosciences) after gel filtration chromatography. The purified protein was buffer-exchanged in crystallization buffer (10 mM Tris-HCl, pH 8.0, 25 mM NaCl, and 0.02% NaN_3), and crystallization experiments were set. For cross-linking experiments, a total of 5 μg of PfUIS3 was incubated with 0.1% of glutaraldehyde for 1 h at room temperature, and the reaction was stopped using Laemmli buffer. The samples were boiled and loaded on SDS-PAGE and visualized using Coomassie staining.

TABLE 1
Data collection and refinement statistics

Data collection	
Space group	$P2_1$
Cell dimensions (Å,°)	a = 82.54, b = 38.27, c = 145.69, and β = 90.25
V_m (Å^3 Da^{-1})	3.41
Solvent content (%)	64.0
Wavelength (Å)	0.9788
Resolution (Å)	25.0-2.5
R_{merge}	0.090 (0.28)
$I/\sigma I$	29.6 (8.1)
Completeness (%)	99.8 (99.4)
Redundancy	9.9 (9.0)
Refinement	
Resolution (Å)	25.0–2.5 (2.50–2.58)
Number of reflections	30,400 (working set, 28,781; test set, 1,619)
R_{work}/R_{free} (%)	22.0/27.0
Protein atoms	5004
Waters	135
PE atoms	300
***B* factor (Å$_2$)**	
Protein	18.6
Waters	18.0
PE atoms	43.5
Stereochemistry	
Root mean square deviation bond length (Å)	0.01
Root mean square deviation bond angle (°)	1.48
Ramachandran plot	
In most favored regions (%)	95.9
In additionally allowed regions (%)	4.1
In disallowed regions (%)	0

Crystallization, Data Collection, and Structure Determination—Selenium-labeled PfUIS3$^{130-229}$ crystals were obtained at 20 °C by hanging drop vapor diffusion method using 1 μl each of PfUIS3$^{130-229}$ (10 mg ml^{-1}) and 0.1 M MES, pH 6.5, 12% polyethylene glycol 20,000, 0.01 M dithiothreitol (mother liquor). A single needle-shaped crystal was flash frozen under a stream of nitrogen gas at 100 K using mother liquor supplemented with 20% glycerol as a cryoprotectant. X-ray diffraction data were collected on a MARCCD detector at the BM14 beam line of the European Synchrotron Radiation Facility. A selenium single-wavelength anomalous dispersion data set to 2.5 Å resolution was collected, and diffraction images were processed and scaled with the HKL2000 suite program (12). All of the 18 expected selenium sites were found, both by AutoSol in Phenix and by SHELXD. PfUIS3$^{130-229}$ crystals are monoclinic and belong to space group $P2_1$ (Table 1). The structure was determined using PHENIX (13) with selenium single-wavelength anomalous dispersion data set. Initial model was built by PHENIX, and this model was subsequently rebuilt using COOT (14). Model refinement was performed using REFMAC (15) without imposing NCS restraints. This was done so that conformations of the six molecules in the asymmetric unit could be determined independently (Table 1). During the course of

model refinement, difference maps showed distinctly Y-shaped electron density (above 2 σ) near Gln^{164} and Glu^{168}. PE molecules were docked into the density, and the complex was refined with REFMAC (15).

Identification of Bound lipids to Purified PfUIS3$^{130-229}$—Bound phospholipids were extracted from pure PfUIS3$^{130-229}$ sample using a chloroform-methanol (2:1) mixture. The organic layer was washed with water and dried under nitrogen. Phospholipid extracts were then resuspended in chloroform:methanol (2:1) mixture. Electron spray ionization analysis was then done in negative polarity mode, which was calibrated externally.

Preparation of Phospholipid Liposome Vesicles—Liposomes were prepared by a sonication method (16) using commercially available lipids. In brief, 1:1.2 molar ratios of 1,2-dipalmitoyl-*sn*-glycero-3-phosphocholine, 1-palmitoyl-2-oleoyl-*sn*-glycero-3-phosphocholine, and cholesterol were used for liposome preparation. The lipid mixture was added to a 50-ml round-bottomed flask and dissolved in diethyl ether, and the system was kept under a stream of nitrogen gas. One-third of the total volume equivalent PBS was added to the above, and the mixture was sonicated briefly to obtain a clear suspension. Subsequently, the organic solvent was evaporated under reduced pressure on a rotatory evaporator. An excess of PBS was added at this stage, and the system was again kept under reduced pressure for 15–20 min so as to remove any traces of organic solvent. The suspension thus obtained was sonicated for 15–20 min on ice, and the resulting clear suspension was filtered through a 0.2-μm Acrodisc syringe filter (PALL Life Sciences) for maintaining homogeneity. These liposomes were characterized by dynamic light scattering and stored at 4 °C.

Circular Dichroism and Dynamic Light Scattering Experiments—For CD analysis of PfUIS3$^{130-229}$-liposomes interactions, the protein was first dialyzed against 5 mM NaH_2PO_4, 5 mM Na_2HPO_4, and 5 mM NaCl, pH 7.0. Far UV spectra (190–240 nm) of PfUIS3$^{130-229}$ (0.1 mg/ml) were recorded at 20 °C in a 1-mm-path length cell with a JASCO-810 spectrophotometer. Scanning speed of 50 nm/min was used, and the instrument was continuously purged with nitrogen to prevent ozone accumulation. The spectra were measured 5-fold and averaged, and the base line was corrected by subtraction of blank buffer. For studying the effect of liposome addition on the overall structure of PfUIS3$^{130-229}$, the liposomes were titrated, and CD spectra were recorded. Bovine serum albumin (BSA), proteinase K, and lysozyme were used as controls. Similarly, freshly prepared liposomes were used for dynamic light scattering analysis using a Photocor-Complex machine at a scattering angle of 90°. Linear correlation function was generated with a sample time of 30 s. Size distribution of liposomes was studied by titrating liposomes with PfUIS3$^{130-229}$. Increasing amounts of PfUIS3$^{130-229}$ protein were added to the liposomes and incubated at 20 °C for 10–15 min. The samples were then analyzed for mean hydrodynamic radius through light scattering. BSA and proteinase K were used as control proteins.

Cloning, Expression, and Purification of Human LFABP—Codon-optimized LFABP (GeneArt) was cloned in PET28a modified vector by using KpnI and NcoI restriction sites and then transformed in *E. coli* B834 host cells. The clones were confirmed by DNA sequencing, and then one was used for inoculation of 10 ml of LB containing ampicillin antibiotic at 37 °C until it reached the log phase. This starter was used as seed culture for inoculation of 1 liter of LB with ampicillin (100 μg/ml). 1 mM isopropyl β-D-thiogalactopyranoside was used for induction of culture at an optical density of 0.6, and the culture was grown at 37 °C for 5 h. Protein was affinity purified using a nickel-chelating column (Pharmacia) and also by gel filtration using a S75 column (Pharmacia).

PfUIS3-LFABP Binding Studies—PfUIS3-LFABP interaction was studied using purified proteins and plate-based ELISAs. 150 ng of purified PfUIS3 was coated on wells of a 96-well microtiter plate in bicarbonate buffer overnight at 4 °C in quadruplicates. The protein gelatin (Sigma) was used as a negative control. After incubation, the plates were washed with PBS, 0.2% Tween 20 (PBST) and blocked with 3% PBS-gelatin (200 μl/well) for 2 h at 37 °C. After blocking, 100 μl of different amounts of His-tagged LFABP (concentrations ranging from 50 to 400 ng) in PBS was used for binding with the plate bound PfUIS3. After 1 h of incubation at 37 °C, extensive washings were done, and the reactions were incubated with 1:4000 dilution of anti-His horseradish peroxidase antibody (Sigma) in 3% gelatin for 1 h at 37 °C. After three more PBST washes, a color reaction was developed using orthophenylenediamine (Sigma) and H_2O_2 in citrate-phosphate buffer. The optical density was measured at 490 nm using an ELISA plate reader (Molecular Probes). An average of four experiments was plotted after deducting background signal from the negative control (Gelatin). Standard deviations were less than 10% in all the cases.

RESULTS

PfUIS3 Production and Oligomeric State—UIS3 gene encoding for residues spanning the PfUIS3 soluble domain (83–229) (without the signal sequence, cytoplasmic tail, and the membrane anchor) was expressed in a bacterial overexpression system. Purified PfUIS3 (residues 83–229) was dimeric in solution as shown by protein cross-linking experiments and gel filtration chromatography (Fig. 1). Dimeric PfUIS3 (residues 83–229) failed to crystallize despite extensive screening; however, a monomeric form (residues 130–229) of PfUIS3 crystallized rapidly. Analysis of the PfUIS3 dimer-monomer transition using gel filtration chromatography and SDS-PAGE suggested that dimeric PfUIS3 underwent proteolysis and reduced to a stable, soluble domain spanning residues 130–229 (Fig. 1*a*). This suggests that residues within residues 83–129 of PfUIS3 are likely to be involved in dimerization of PfUIS3. From here on, this soluble domain will be referred to as PfUIS3$^{130-229}$.

Overall Structure of PfUIS3$^{130-229}$—We determined the crystal structure of soluble PfUIS3$^{130-229}$ by collecting single-wavelength anomalous dispersion data from selenium-labeled protein. Initial electron density map calculation and model refinement were done at 2.5 Å resolution. PfUIS3$^{130-229}$ crystals contain six molecules/asymmetric unit, and the volume per asymmetric unit is V_M 3.41 $Å^3$ Da^{-1}, which is equivalent to a solvent content of 64%. The refined structure for PfUIS3$^{130-229}$-PE complex has R_{work} and R_{free} values of 22 and 27%, respectively (Table 1). The refined model has excellent stereochemistry and contains 135 water molecules and six PE

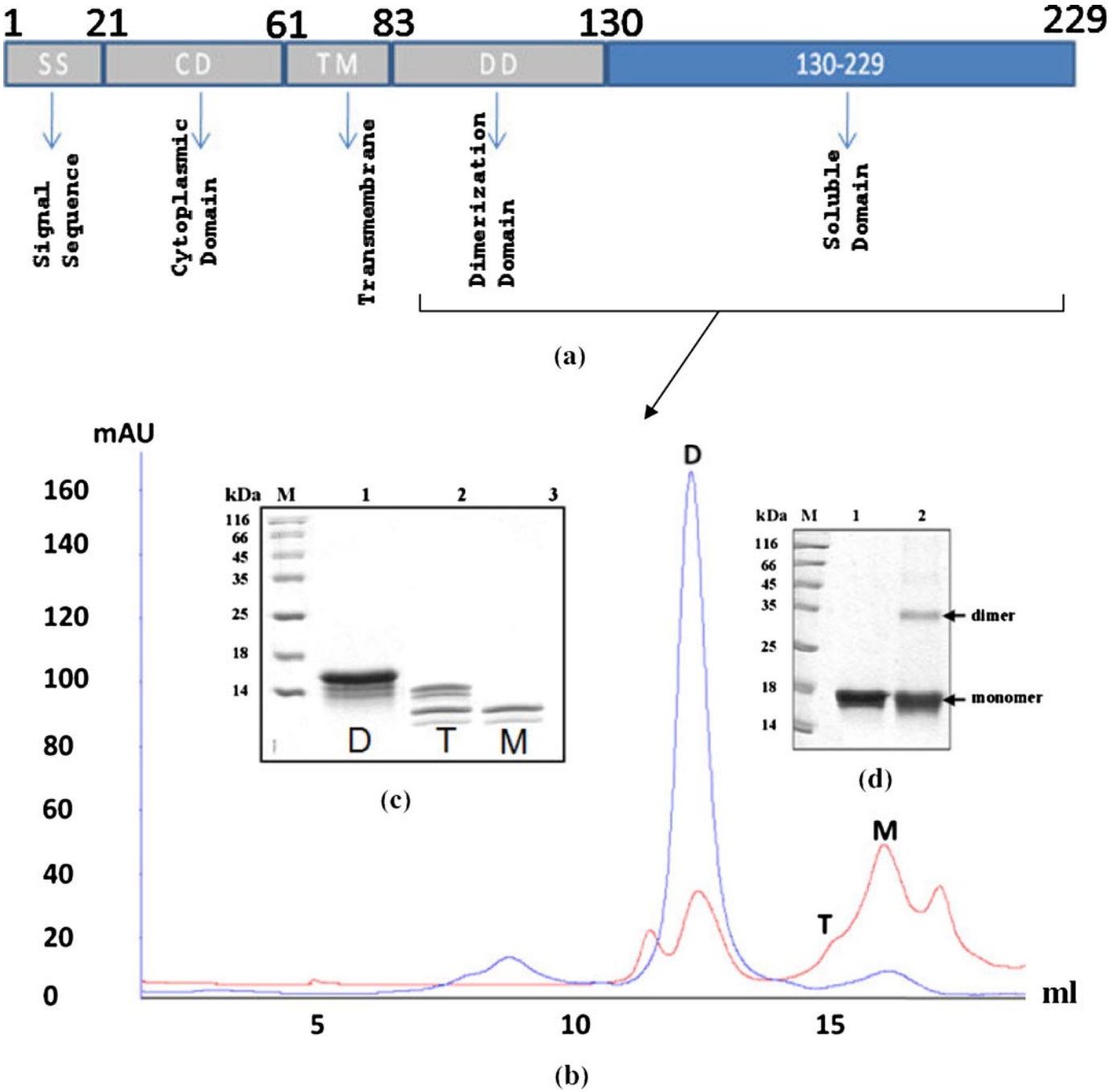

FIGURE 1. *a*, domain representation of PfUIS3. *b*, soluble domain of PfUIS3 is dimeric in solution. Superdex 75 gel filtration analysis of PfUIS3 reveals the existence of dimers (*blue*) and monomers (*red*). *c*, SDS-PAGE of the fractions *D*, *T*, and *M* indicating truncation of the PfUIS3 construct from residues 89–229 (dimeric) to residues 130–229 (monomeric in nature). *d*, SDS-PAGE analysis of glutaraldehyde cross-linking (0.1%) control PfUIS3 (*lane 1*) and glutaraldehyde cross-linked PfUIS3 (*lane 2*). PfUIS3 at a concentration of 4 mg ml^{-1} was used for gel-filtration and cross-linking experiments.

molecules. Data processing and refinement statistics are summarized in Table 1.

The superposition of C^{α} atoms of the six monomers (A to F) of $PfUIS3^{130-229}$ in the asymmetric unit gives an root mean square deviation of ~0.5 Å. There is no noncrystallographic point group symmetry found between the six $PfUIS3^{130-229}$ protomers. Interestingly, the protomer arrangements reveal two independent helical motifs (-A-C-F-A-C-F- and -B-D-E-B-D-E-) along the crystallographic *b*-axis. The thickness of the helix is ~67 Å with inner and outer diameters of ~43 and ~110 Å, respectively. $PfUIS3^{130-229}$ monomers AB, CD, EE′, and FF′ are related by ~180° (E′ and F′ are symmetry equivalent molecules). There are two different sets of intermolecular interactions: (*a*) between A and B, C and D, E and E′, and F and F′ and (*b*) between B and E and D and F. PfUIS3 has dimensions of ~44 × 29 × 23 Å and adopts a globular fold of four α-helices that pack against each other tightly. Residues from 130–148 form a random coil (C1) at the N terminus, and this is followed by an α-helix (H1, residues 149–169). A tight turn T1 (170–171) separates α-helix H2 (172–178) from α-helix H1. Another

turn T2 (179–181) connects α-helix H2 with α-helix H3 (182–196). Finally, turn T3 (197–201) connects α-helix H3 to terminal α-helix H4 (202–227) (Fig. 2). PfUIS3$^{130-229}$ fold is highly reminiscent of the ubiquitous helix-turn-helix motifs, and sequence comparison of UIS3 homologs from various plasmodial species suggests a high level of conservation (Fig. 3). The PfUIS3 surface has a spatially distinct opposite charge character. A broad negatively charged patch is evident on one face of PfUIS3$^{130-229}$, which contains many charged residues, particularly Glu^{228}, Glu^{227}, Asp^{176}, and Asp^{173} (Fig. 4*a*). Distal to this acidic cluster is a channel of basic residues: Lys^{150}, Arg^{151}, Arg^{196}, Lys^{165}, and Lys^{131} (Fig. 4*b*).

PE Forms a 1:1 Complex with PfUIS3$^{130-229}$—During model refinement of PfUIS3$^{130-229}$, difference electron density maps revealed regions of elongated Y-shaped electron density near residues Glu^{166}, Gln^{168}, Asn^{222}, and Asn^{226} and between H1 and H4 helices close to the surface of PfUIS3$^{130-229}$. The shape of the extra surface electron density (contoured at 2.0 and 1.0 σ levels for $F_o - F_c$ and $2F_o - F_c$, respectively; Fig. 5*a*) immediately suggested a potential lipid/fatty acid interaction. An in-depth analysis of this extra density, including docking of fatty acids and lipids, suggested that only lipids such as PE and phosphatidylcholine satisfactorily docked into the distinctly Y-shaped electron density (Fig. 5*a*). The presence of bound ligands was tested by tandem MS analysis of purified crystallization grade PfUIS3$^{130-229}$. The phospholipid range in time-of-flight MS analysis was between 680 and 780 daltons. The shown tandem MS analysis of 716 daltons at collision energy 40 eV for 5 min shows expected fragments of PE. These data indicated the presence of 1-palmitoyl-2-oleoyl-phosphatidylethanolamine at a molecular size of 716 daltons (Fig. 5*b*) bound to PfUIS3$^{130-229}$. This is consistent with the fact that phosphatidylethanolamine is an abundant lipid of *E. coli* and constitutes ~75% of membrane lipids (17). Given that PfUIS3 was overexpressed in *E. coli*, it is therefore likely that PE was nat-

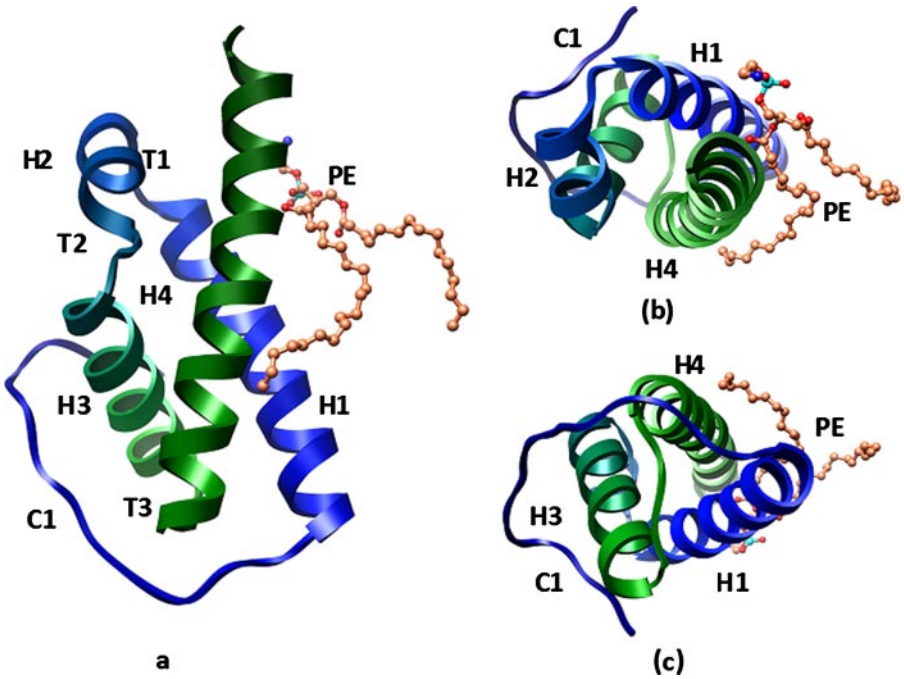

FIGURE 2. *a*, the overall domain architecture and crystal structure of the PfUIS3$^{130-229}$-PE complex. The protein is colored from *blue* to *green* as the chain traverses from the N to the C termini. PfUIS3 is a compact structure consisting of four α-helices H1 (residues 149–169), H2 (residues 174–176), H3 (residues 182–196), and H4 (residues 202–228) and an N-terminal coiled structure (residues 130–148). Bound PE is colored *orange* and shown as ball-and-stick. *b*, view of the PfUIS3$^{130-229}$-PE complex. *c*, orthogonal view of the PfUIS3$^{130-229}$-PE complex.

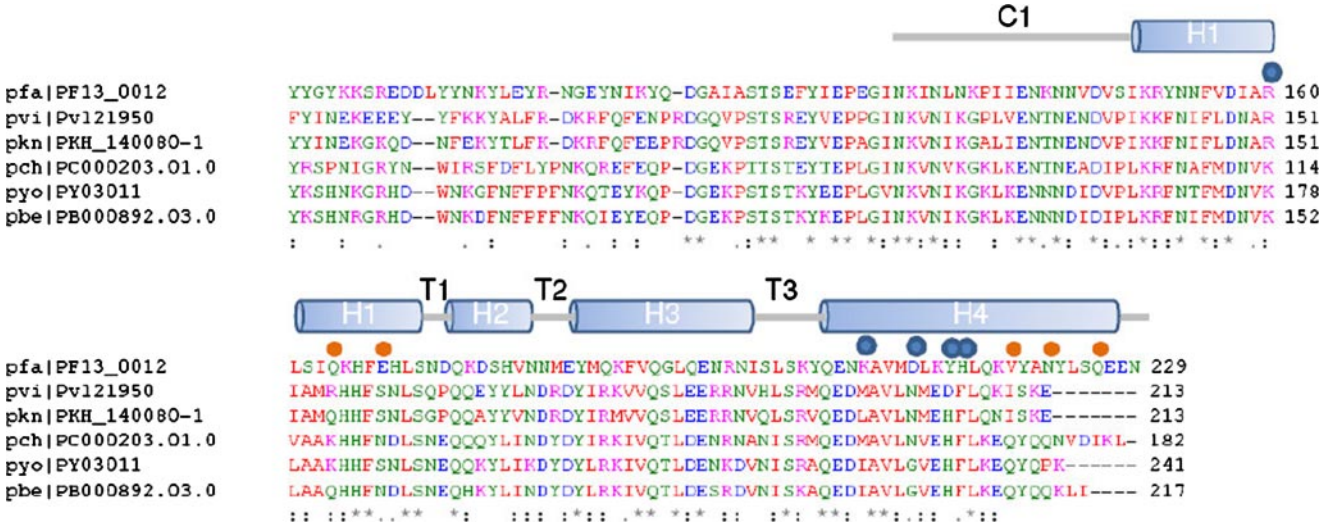

FIGURE 3. **Sequence alignment of PfUIS3 with homologs from malaria parasites.** *pfa*, *Plasmodium falciparum*; *pvi*, *Plasmodium vivax*; *pkn*, *Plasmodium knowlesi*; *pch*, *Plasmodium chabaudi*; *pyo*, *Plasmodium yoelii*; *pbe*, *Plasmodium berghei*. The sequence alignment is for the soluble region of UIS3, which is exposed to the hepatocyte cytoplasm. The structural features are indicated above the sequence. The *orange dots* and *blue dots* above the sequence highlight residues involved in PE head group interactions and in lining of the hydrophobic cavity.

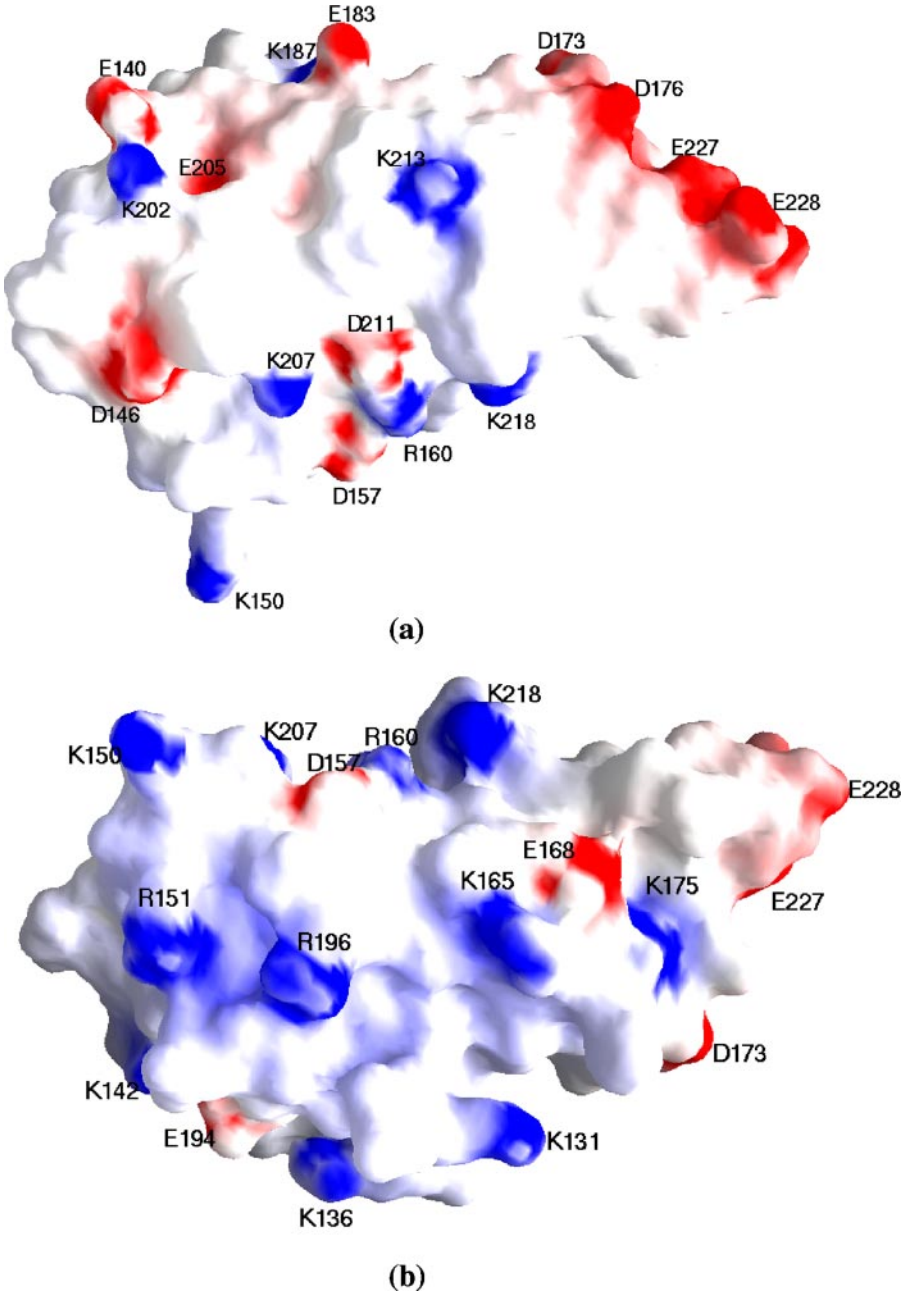

FIGURE 4. **Distinctly dual charge character of PfUIS3$^{130-229}$.** *a* and *b*, electrostatic surface representation of PfUIS3 in orthogonal views showing the negative charge patch (*a*) and the conserved positively charged cluster (*b*). The surface is colored *blue* for potentials >10 kT/e and *red* for potentials < −10 kT/e.

urally bound during *UIS3* overproduction within the bacterial cell, as has been found in many previous studies of fatty acid-binding proteins. Confirmation of ligand identity by mass spectrometry allowed us to model PE molecules into the extra density on the surface of PfUIS3$^{130-229}$. Structure of PE (Protein Data Bank entry 1lqv) shows a remarkable fit in the Y-shaped density and makes close contacts with side chains emanating from PfUIS3$^{130-229}$ (Figs. 5*a* and 6). We were able to model PE phosphate head groups for each of the six monomers of PfUIS3$^{130-229}$ in the asymmetric unit. The excellent quality of difference and $2F_o - F_c$ maps allowed us to model three complete and three partial chains of PE. The models were refined using crystallographic data to 2.5 Å resolution, and R_{free} was monitored throughout the course of model building and refinement of the PfUIS3$^{130-229}$-PE complex described here.

PfUIS3$^{130-229}$ forms a 1:1 complex with phosphatidylethanolamine as is evident from the structure (Fig. 6). The phosphate head group of the PE molecules is stabilized by hydrogen bonds with numerous protein side chains including those of Gln^{164}, Glu^{168}, Asn^{222}, and Asn^{226} (Fig. 6*c*). These residues participate in hydrogen bonds to stabilize the phosphate head group of PE (Fig. 6*c*). The nitrogen atom of the ethanolamine group interacts with O$^{\delta1}$ of the Asn^{226} from PfUIS3 (Fig. 6*c*). In addition, the PE head group is interacting with backbone polar atoms of Val^{219} and Tyr^{223} via structural water molecule (Fig. 6*c*). This particular water is conserved in all PfUIS3$^{130-229}$-PE interfaces, and it contributes stabilizing hydrogen bonding interactions. Mapping of the PE footprint on PfUIS3$^{130-229}$ highlights a narrow, surface-exposed, hydrophobic channel that accommodates one acyl chain of PE (Fig. 6*a*). One end of this channel is polar and makes a binding site for zwitterionic head group of phospholipids PE (Fig. 6*b*). This binding site resides between helices H1 and H4 with an accessible surface area of 914 Å^2. The volume enclosed by this hydrophobic gateway is 449.5 Å^3, large enough to accommodate a variety of fatty acid and lipid apolar chains. One of the hydrophobic PE chain fits exceedingly well in the apolar cavity of PfUIS3$^{130-229}$ (Fig. 6*b*). Proximal to the hydrophobic channel there are four positively (Lys^{207}, His^{215}, Lys^{218}, and Arg^{160}) and one negatively (Asp^{211}) charged residue, in addition to a salt bridge between Arg^{160} and Asp^{211} (Fig. 6*d*). These polar residues are engaged in hydrogen-bonding networks, and their hydrophobic stems seem to provide the apolar environment for acceptance of the PE acyl chain. Closer inspection of above interactions (using reference chain C of PfUIS3$^{130-229}$) reveals the following: (*a*) the N$^{\epsilon2}$ of His^{215} hydrogen bonds with O$^{\epsilon1}$ of Gln^{164}, (*b*) N$^{\delta1}$ of His215 hydrogen bonds with water W113, (*c*) the NE and NH1 of Arg160 hydrogen bonds with O$^{\delta1}$/O$^{\delta2}$ of Asp^{211}, Trp^{76}, and Trp^{113}, and finally, (*d*) the NZ of Lys^{207} hydrogen bonds with water Trp^{74} (Fig. 6*d*). Residues Met^{182}, Met^{210}, and Lys^{213} of

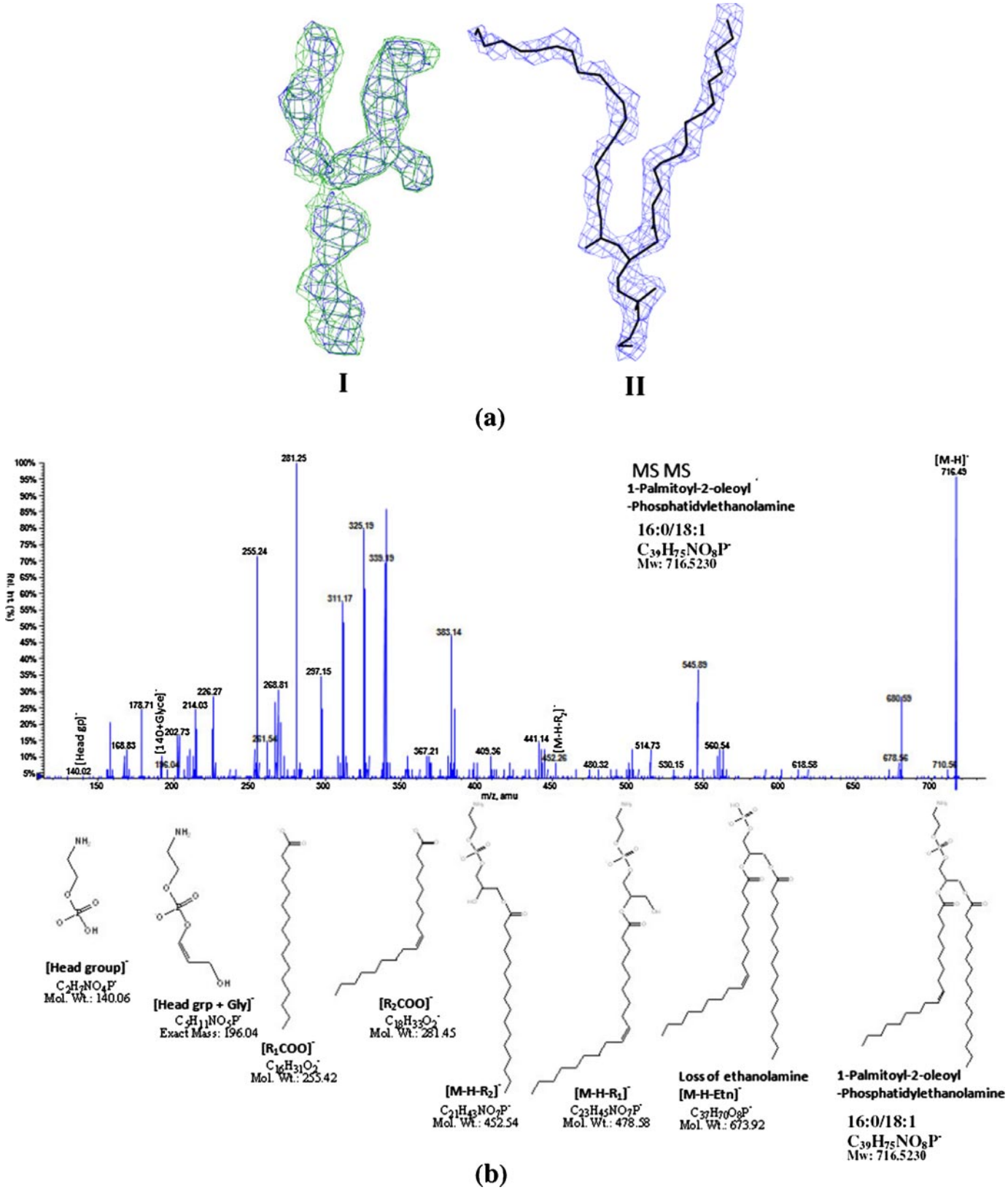

FIGURE 5. **Lipid electron density in PfUIS3$^{130-229}$-PE complex.** *a*, distinctly Y-shaped electron density was observed in difference maps during the model refinement of PfUIS3$^{130-229}$. The electron density maps shown are contoured at 2.0 σ (*green*) and 1.0 σ (*blue*) for $F_o - F_c$ and $2F_o - F_c$, respectively. A molecule of PE was fit into the additional Y-shaped density observed. The final $2F_o - F_c$ map is contoured at a 1.0 σ level. *b*, tandem MS analysis of bound PEs extracted from PfUIS3$^{130-229}$.

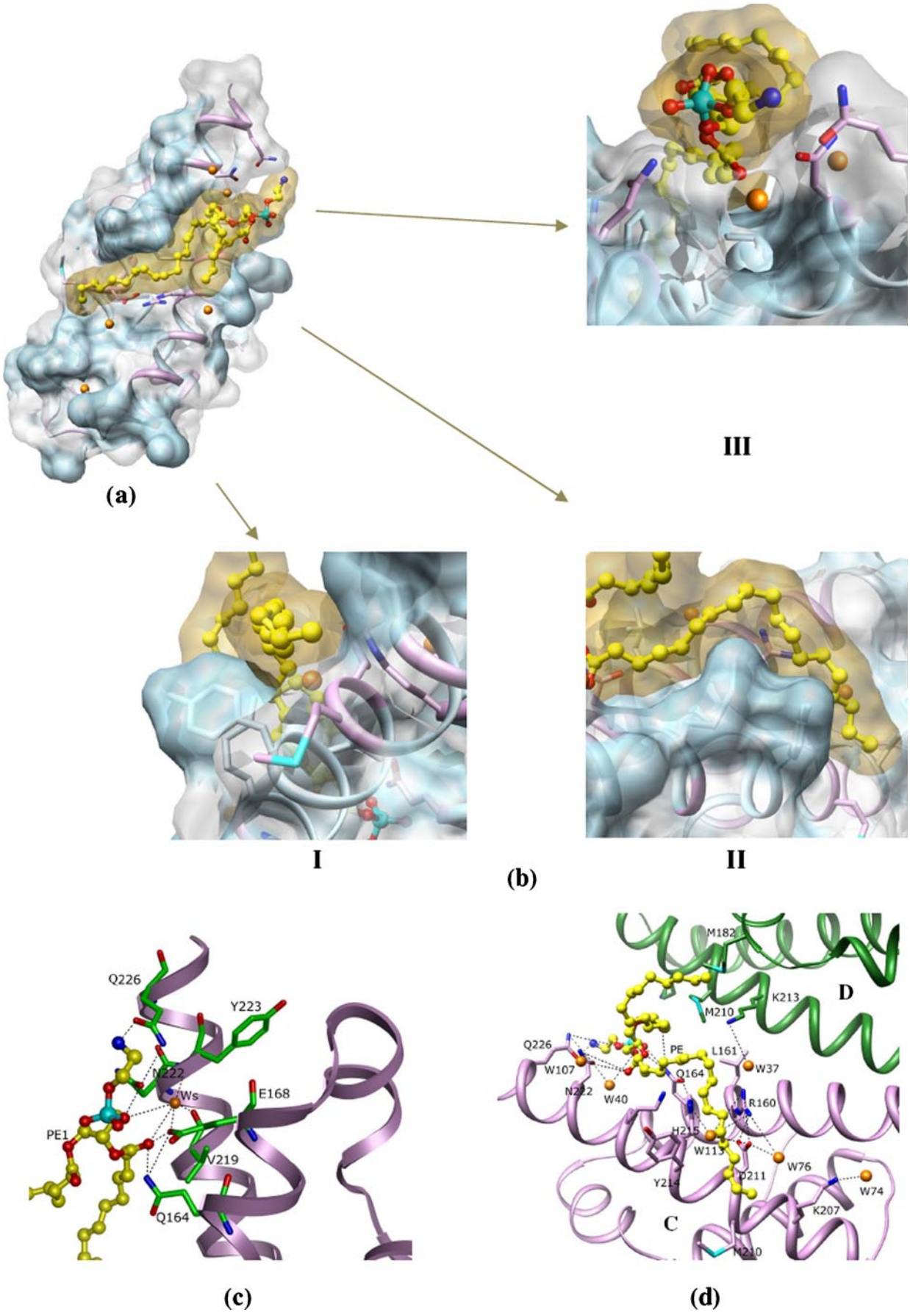
(a)
III
I
II
(b)
Q226
Y223
N222
Ws
E168
PE1
V219
Q164
(c)
M182
K213
D
M210
Q226
PE
L161
W107
Q164
W37
N222
W40
R160
H215
W113
W76
D211
Y214
W74
K207
C
K210
(d)

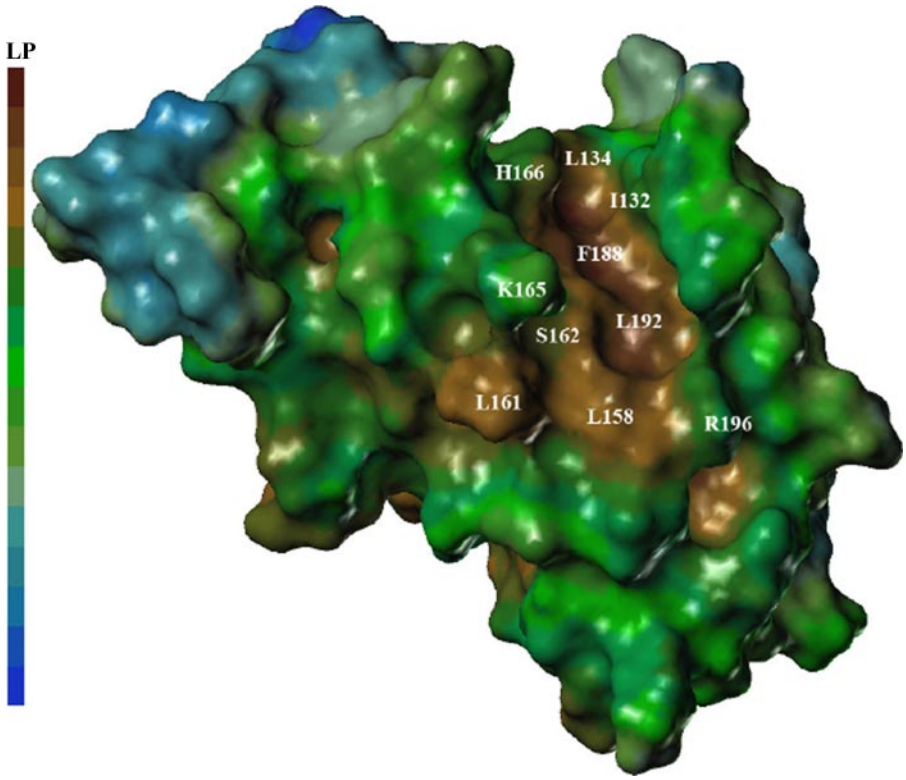

FIGURE 7. **Lipophilic surface representation of PfUIS3.** The surface is color-coded from *dark brown* to *blue* according to its lipophilic nature. A hydrophobic cavity is present on the surface that is lined largely by conserved hydrophobic residues.

neighboring PfUIS3$^{130-229}$ chain seem to stabilize the second acyl chain of PE (Fig. 6*d*).

Surface lipophilicity analysis of PfUIS3 reveals the presence of a lipophilic channel very near to PE binding channel (Fig. 7).This channel is lined by residues Leu^{134}, Ile^{132}, Phe^{188}, Leu^{192}, Leu^{158}, and Leu^{161}, which are largely conserved in all the plasmodial UIS3. The biological significance of this channel is not fully clear, but it seems that it may also act as a binding site for hydrophobic cargo.

PfUIS3$^{130-229}$ residues that make close contact with the PE head group show some degree of sequence conservation in *Plasmodial* UIS3s, specifically, in a conserved ability to participate in network of hydrogen bonds (Fig. 3). It may be that PfUIS3 family members have necessarily limited capacity to differentiate between various lipids and fatty acids; UIS3 proteins may act as generic fatty acid/lipid adaptors with the general ability to recognize and bind a variety of lipid-like cargo that the growing parasite might require. This lack of specificity will manifest itself in limited sequence conservation that will therefore allow a wider array of lipid-like ligands to be bound and transported.

PfUIS3$^{130-229}$ Interaction with Fatty Acids and Liposomes—PfUIS3$^{130-229}$-lipid/fatty acid interactions were further probed using two independent biophysical techniques. We performed CD experiments using far UV (240–190 nm) on purified PfUIS3$^{130-229}$ (monomer)-liposome complexes. A titration study indicated distinct and specific conformational changes in PfUIS3$^{130-229}$ in the presence of liposomes (Fig. 8*a*). Interaction with liposomes seems to decrease the helical content of PfUIS3$^{130-229}$ in favor of random coil (Fig. 8, *a* and *b*), suggesting increased disorder in the protein. A plot of ellipticity as a function of liposome concentration at 208 nm (Fig. 8*c*) and 222 nm (Fig. 7*d*) emphasizes this conformational shift. To probe whether PfUIS3$^{130-229}$ interaction with liposomes resulted in sequestration of PfUIS3$^{130-229}$ onto liposomes, we used dynamic light scattering as a probe of molecular size distribution in PfUIS3$^{130-229}$-liposome complexes. As shown in Fig. 9, an increase in the hydrodynamic radius of liposomes was observed as a function of PfUIS3$^{130-229}$ concentration. Enlargement of liposome upon PfUIS3$^{130-229}$ engagement indicates specific complex formation between the two and possible sequestration of multiple molecules of PfUIS3$^{130-229}$ on the liposome surface. Such liposome decoration with PfUIS3$^{130-229}$ may mimic the interaction of PfUIS3$^{130-229}$ with parasite PVM, an event likely to facilitate transfer of fatty acid/lipid cargo directly on to the parasite membrane.

PfUIS3$^{130-229}$ Binds Human Liver Fatty Acid-binding Protein—The rodent malaria parasite homolog of PfUIS3, PyUIS3, is known to interact with mouse liver fatty acid-binding protein as shown previously by yeast two-hybrid screens and co-immunoprecipitation experiments (4). Not surprisingly, we found that the homolog of PyUIS3 in *P. falciparum* interacts with the human counterpart of rodent LFABP. Our evidence for PfUIS3$^{130-229}$-human FABP interaction is based on purified components used in protein-protein based ELISAs (Fig. 10). The binding between PfUIS3$^{130-229}$ and human LFABP was specific and dose-dependent. Further, this experiment clearly suggests that the recognition site for human LFABL on PfUIS3 resides within the monomeric 130–229 spanning domain.

DISCUSSION

Recent genomic data on malaria parasite liver stages provide a new rationale for the development of sporozoite-spe-

FIGURE 6. **Surface representation and hydrogen bonding interactions in PfUIS3$^{130-229}$-PE complex.** *a*, hydrophobic portion of PfUIS3$^{130-229}$ and bound PE molecule are colored *light blue* and *yellow*, respectively. *b*, view of PE on the surface of PfUIS3$^{130-229}$showing close atomic interactions. *Panel I*, snapshot of end of one acyl chain of PE in the PfUIS3 hydrophobic channel. *Panel II*, one acyl chain of PE interacts mostly with hydrophobic residues or hydrophobic stems of polar residues and the lipid wraps around PfUIS3$^{130-229}$. *Panel III*, the head group of PE makes close contacts with polar residues and with one conserved water molecule (colored *orange*) *c* and *d*, views of the interactions between zwitterionic head group of PE and PfUIS3 surface residues. The highly ordered water molecule (*W61*) is colored *orange*.

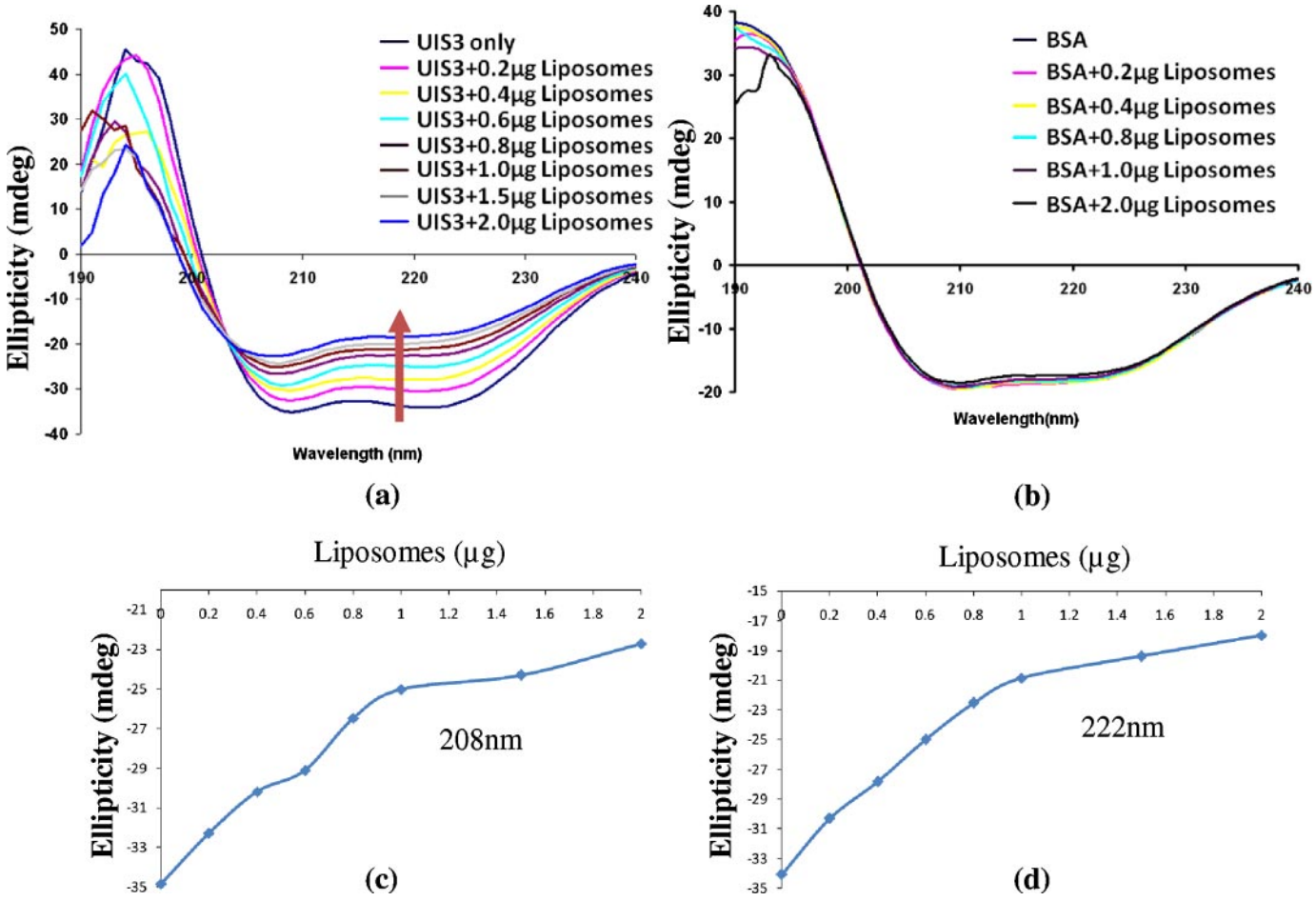

FIGURE 8. **CD analysis of PfUIS3$^{130-229}$-liposome complexes.** *a*, CD spectra (240–190 nm) of PfUI3 as a function of liposome concentration. Different amounts of phospholipid liposomes were used (ranging from 0.2 to 2.0 μg) in these experiments, while PfUIS3$^{130-229}$ was kept constant. The *colored lines* indicate spectra in the presence of different concentrations of phospholipid vesicles. Upon titration of liposomes, distinct changes in the CD moments of PfUIS3$^{130-229}$ spectra were observed implying conformational changes. *b*, CD spectra of BSA under similar conditions. *c* and *d*, the conformational changes in PfUIS3$^{130-229}$ as a function of liposome concentration as probed by monitoring change in ellipticity at 202 nm (*c*) and at 222 nm (*d*).

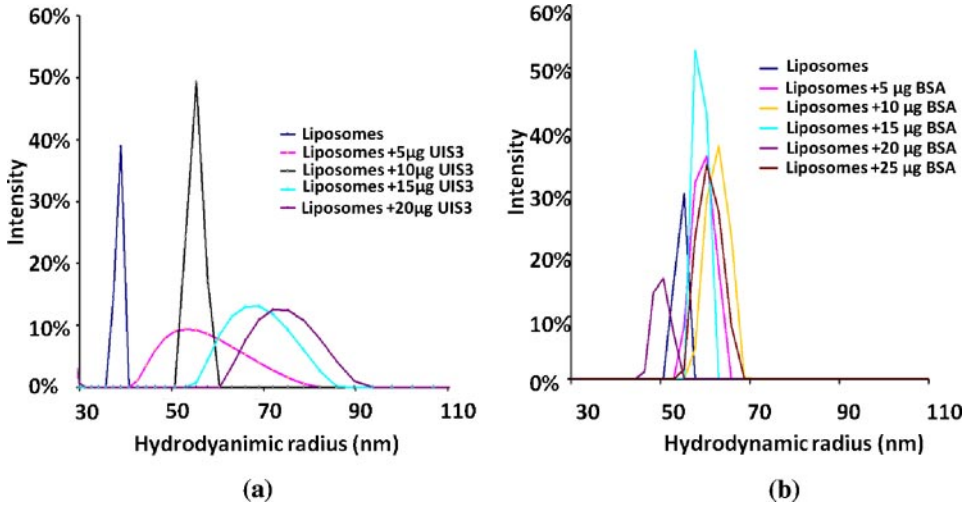

FIGURE 9. **Dynamic light scattering studies of PfUIS3$^{130-229}$-liposome complexes.** *a*, a distinct increase in the hydrodynamic radii of liposomes was observed with the addition of PfUIS3$^{130-229}$ indicating assembly and decoration of liposomes with PfUIS3$^{130-229}$. *b*, no such shift in molecular size of liposomes was observed with control proteins like BSA (and others; data not shown).

cific inhibitors that abrogate malaria infection in the liver. After sporozoite invasion of the host liver cell, molecular components from the latter are used for synthesis of vital parasite structural features like the parasitophorous vacuolar membrane (5). Although the malaria parasite is able to synthesize fatty acids through an apicoplast-based biosynthesis pathway (18), it seems that during hepatocytic stages, the parasite relies on host fatty acids for rapid synthesis of its membranes (4, 18). A host of proteins (like *UIS3*) are therefore inserted in the PVM to enable import of essential nutrients (4, 19). Genetic interference with these transport pathways is often deleterious to the parasite, as has been already shown for *UIS3*- and *UIS4*-deficient parasites (3). UIS3 is a membrane protein with distinct transmembrane and soluble domains. Sequence analysis of PfUIS3 suggests that residues 1–21 form its signal sequence, residues 22–59 entail the cytosolic region, whereas its transmembrane region is

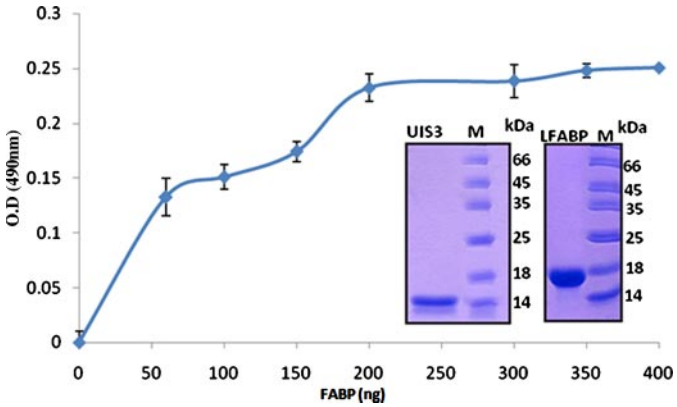

FIGURE 10. **Binding of PfUIS3$^{130-229}$ to human LFABP.** Protein-protein based ELISAs were performed as described under "Experimental Procedures." Each experiment was performed in quadruplicate, and an average of four experiments was plotted after deducting the background signal from the negative control (Gelatin). The standard deviations were less than 10% in all cases. SDS-PAGE of purified PfUIS3 and LFABP used in these ELISAs are shown as *insets* in the figure.

formed by residues 60–83 (3). The overall domain architecture of PfUIS3 suggests that the soluble region of PfUIS3 (89–229) is exposed to the contents of the hepatocyte cytoplasm. Our biochemical data indicate that the PfUIS3 region spanning residues 89–229 is soluble and dimeric in solution, whereas truncation of PfUIS3 to the 130–229 segment abolishes its dimerization property. The oligomerization domain is therefore contained within the region from residues 89 to 129 and indicates that PfUIS3 exists as two subdomains, a dimerization subdomain (residues 89–129) and a large four-helical bundle subdomain (residues 130–229).

We solved the crystal structure of PfUIS3$^{130-229}$ in complex with a bound phospholipid molecule. The surface of PfUIS3$^{130-229}$ has spatially distinct areas of positive and negative charge density, and it displays a hydrophobic channel where one acyl arm of PE is able to bind (Figs. 5 and 6). The phosphate head group of bound PE in PfUIS3$^{130-229}$-PE complex structure forms specific hydrogen bonding interactions with several polar residues at one end of hydrophobic channel. A conserved water molecule is also involved in these interactions (Fig. 6). The architecture of this binding site hints that a large repertoire of phospholipid/fatty acid molecules can bind in this cavity because only residues interacting with the phosphate head group of PE were conserved in their characteristics of forming hydrogen bond networks. Aside from these structural insights, two sets of biophysical experiments using liposomes and pure PfUIS3$^{130-229}$ clearly highlight the ability of PfUIS3$^{130-229}$ to form specific complexes with liposomes and conformational changes in PfUIS3$^{130-229}$ upon binding of liposomes. We also studied the direct interaction of PfUIS3$^{130-229}$ with human LFABP, which is in agreement with the previous findings with the rodent homolog of PfUIS3 (4).

Our present study provides crucial evidence that PfUIS3 may itself act as a fatty acids/lipid carrier given that it is capable of interacting directly with phospholipids and liposomes. This ability of PfUIS3 is in addition to its interaction with LFABP. Therefore, PfUIS3 may participate in lipid exchange by sequestering the FABP cargo for forward passage to the membrane on which PfUIS3 resides. A stepwise mechanism probably exists where fatty acid/lipids carried by LFABP are initially transferred to PfUIS3, which subsequently delivers them to the PVM, from where they may be internalized into the parasite. The region of PfUIS3 from residues 83 to 129 is predicted to be random coiled coil, which is known to be flexible. This linker region might provide a flexible hinge for interaction of PfUIS3$^{130-229}$-PE-FABP complex with the PVM. Our structural and functional data provide new insights into the role of PfUIS3 in the transfer of hydrophobic cargo from host cytoplasm/FABP to and through the parasite PVM.

Within the family of well characterized FABPs, those capable of "collisional transfer" (like the intestinal FABP) can interact directly with membranes during fatty acid transfer (22). The α-helix (α1) of collisional FABPs is amphipathic in nature and may assist in lipid transfer. On the other hand, liver FABPs do not employ collisional mechanism of fatty acid transfer (10, 20). An analysis of surface electrostatic potentials for several FABPs demonstrates a net positive potential across the helix-turn-helix portal region of colliosional transfer FABPs, which supports the suggestion that this region is involved in interaction with membranes (10, 21, 22). On the other hand, human liver FABP contains three conserved acidic residues that emanate from its helix turn helix portal and form a distinct negative patch on its surface from where fatty acid shuttling is likely to be triggered (23). However, the liver FABPs are inefficient at transferring fatty acids/lipids to membranes and may therefore require additional protein adaptors (like PfUIS3) to assist in unloading of lipid-like luggage on to the membrane network. These insights underpin the significance of both LFABP and PfUIS3 in lipid/fatty acid ingress for the parasite. We propose that liver FABPs may interact with UIS3s in a dynamic and continuous process of cargo transfer. This scenario is in contrast to FABPs of the intestinal variety that employ the collisional transfer mechanism and are therefore more efficient at off-loading their ligands directly to membranes, without protein or molecular intermediaries.

In the aqueous environment of the liver hepatocyte cytosol, the presence of free fatty acids is unlikely because of their hydrophobic character. The parasite seems to have therefore developed molecular machinery that can act as a conduit for stepwise capture and transfer of fatty acid, thereby obviating the requirement for extensive lipid synthesis within the parasite. The likely mechanism of interaction (Fig. 11), based on structures of LFABP and PfUIS3$^{130-229}$ may be: (*a*) LFABP shuttles fatty acids/lipids from host cytoplasm to UIS3, (*b*) UIS3 binds directly to LFABP and captures its cargo in a continuous and dynamic fashion, (*c*) UIS3 ligand-binding sites undergo conformational changes to accommodate fatty acids/lipids, and finally, (*d*) similar to the collisional transfer mechanism used by other fatty acid transporters, the membrane tethered UIS3 releases its cargo directly on to the parasite PVM. Repetition of this transfer cycle will ensure a ready supply of LFABP cargo to the growing parasite within the host liver

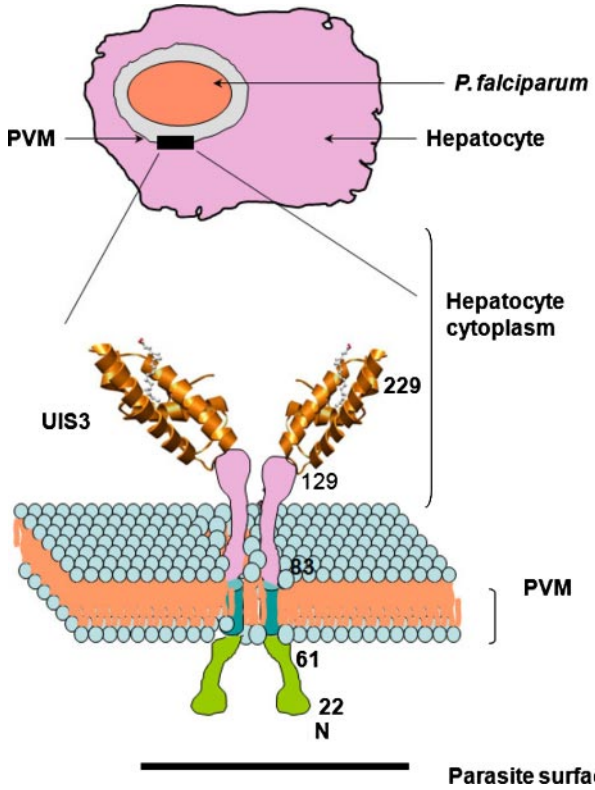

FIGURE 11. **Model of molecular cross-talk between PfUIS3 and fatty acids/lipids.** PfUIS3 is resident on the PVM, and its larger, soluble domain is exposed to the contents of the hepatocyte cytoplasm. PfUIS3$^{130-229}$ adopts a four α-helix bundle that cannot only bind to LFABP but also directly interact with lipids. These twin abilities suggest that PfUIS3 may be a critical molecular motor for lipid import into the parasite.

cell; the absence of UIS3 therefore robs the parasite of a molecular intermediary capable of scavenging LFABP cargo.

It seems feasible to specifically block the interaction of fatty acids/lipids with their carrier proteins using small molecule inhibitors (24). This has been recently been shown by development of human fatty acid-binding-protein aP2 inhibitors, which may be useful in treatment of diabetes and atherosclerosis (24). Our high resolution structural analysis of PfUIS3$^{130-229}$-PE complex provides a structural framework for initiating development of small molecule mimics that can target molecular functions of PfUIS3. Disruption of PfUIS3 interactions with lipids/fatty acids/FABP by employment of molecular agents may lead to developmental arrest of sporozoites in the host liver. Such inhibitory agents may serve as prophylactics and prevent egress of malaria parasites from the infected liver. Inhibiting molecular functions of UIS3 may therefore target malaria parasite before the initiation of erythrocytic stages, prior to the onset of symptomatic malaria.

Acknowledgments—We thank all past and present members of the International Centre for Genetic Engineering and Biotechnology. We are grateful to Madhusudan and Dr. Rajesh Gokhale of the National Institute of Immunology (New Delhi) for mass spectrometry data analysis. We also thank Aseem Mishra for assistance with CD and dynamic light scattering experiments. Finally, we thank Hassan Belrhali for assistance with data collection at BM14, ESRF, France.

REFERENCES

1. Snow, R. W., Guerra, C. A., Noor, A. M., Myint, H. Y., and Hay, S. I. (2005) *Nature* **434,** 214–217
2. Kaiser, K., Matuschewski, K., Camargo, N., Ross, J., and Kappe, S. H. (2004) *Mol. Microbiol.* **51,** 1221–1232
3. Mueller, A. K., Labaied, M., Kappe, S. H., and Matuschewski, K. (2005) *Nature* **433,** 164–167
4. Mikolajczak, S. A., Jacobs-Lorena, V., MacKellar, D. C., Camargo, N., and Kappe, S. H. (2007) *Int. J. Parasitol.* **37,** 483–489
5. Lingelbach, K., and Joiner, K. A. (1998) *J. Cell Sci.* **111,** 1467–1475
6. Thompson, J., Reese-Wagoner, A., and Banaszak, L. (1999) *Biochim. Biophys. Acta* **1441,** 117–130
7. Ockner, R. K., Manning, J. A., Poppenhausen, R. B., and Ho, W. K. (1972) *Science* **177,** 56–58
8. Storch, J. (1993) *Mol. Cell Biochem.* **123,** 45–53
9. Levi, A. J., Gatmaitan, Z., and Arias, I. M. (1969) *J. Clin. Investig.* **48,** 2156–2167
10. Falomir-Lockhart, L. J., Laborde, L., Kahn, P. C., Storch, J., and Corsico, B. (2006) *J. Biol. Chem.* **281,** 13979–13989
11. Hendrickson, W. A., Horton, J. R., and LeMaster, D. M. (1990) *EMBO J.* **9,** 1665–1672
12. Otwinowski, Z., and Minor, W. (1997) *Methods Enzymol.* **276,** 307–326
13. Adams, P. D., Grosse-Kunstleve, R. W., Hung, L. W., Ioerger, T. R., McCoy, A. J., Moriarty, N. W., Read, R. J., Sacchettini, J. C., Sauter, N. K., and Terwilliger, T. C. (2002) *Acta Crystallogr. Sect. D Biol. Crystallogr.* **58,** 1948–1954
14. Emsley, P., and Cowtan, K. (2004) *Acta Crystallogr. Sect. D Biol. Crystallogr.* **60,** 2126–2132
15. Murshudov, G. N., Vagin, A. A., and Dodson, E. J. (1997) *Acta Crystallogr. Sect. D Biol. Crystallogr.* **53,** 240–255
16. Szoka, F., Jr., and Papahadjopoulos, D. (1978) *Proc. Natl. Acad. Sci. U. S. A.* **75,** 4194–4198
17. Morein, S., Andersson, A., Rilfors, L., and Lindblom, G. (1996) *J. Biol. Chem.* **271,** 6801–6809
18. Ralph, S. A., van Dooren, G. G., Waller, R. F., Crawford, M. J., Fraunholz, M. J., Foth, B. J., Tonkin, C. J., Roos, D. S., and McFadden, G. I. (2004) *Nat. Rev. Microbiol.* **2,** 203–216
19. Lingelbach, K. R. (1993) *Exp. Parasitol.* **76,** 318–327
20. Thumser, A. E., and Storch, J. (2000) *J. Lipid Res.* **41,** 647–656
21. Di Pietro, S. M., Corsico, B., Perduca, M., Monaco, H. L., and Santome, J. A. (2003) *Biochemistry* **42,** 8192–8203
22. LiCata, V. J., and Bernlohr, D. A. (1998) *Proteins* **33,** 577–589
23. Hodsdon, M. E., and Cistola, D. P. (1997) *Biochemistry* **36,** 1450–1460
24. Furuhashi, M., Tuncman, G., Gorgun, C. Z., Makowski, L., Atsumi, G., Vaillancourt, E., Kono, K., Babaev, V. R., Fazio, S., Linton, M. F., Sulsky, R., Robl, J. A., Parker, R. A., and Hotamisligil, G. S. (2007) *Nature* **447,** 959–965